NASA TECHNICAL MEMORANDUM

NASA TM X-68294

NASA TM X-68294

PERFORMANCE OF 30-CM ION THRUSTERS WITH DISHED ACCELERATOR GRIDS

by Vincent K. Rawlin
Lewis Research Center
Cleveland, Ohio 44135

TECHNICAL PAPER proposed for presentation at
Tenth Electric Propulsion Conference sponsored
by the American Institute of Aeronautics and Astronautics
Lake Tahoe, Nevada, October 31 - November 2, 1973

PERFORMANCE OF 30-CM ION THRUSTERS WITH DISHED ACCELERATOR GRIDS

Vincent K. Rawlin
National Aeronautics and Space Administration
Lewis Research Center
Cleveland, Ohio

Abstract

Thirteen sets of dished accelerator grids were tested on five different 30-cm diameter bombardment thrusters to evaluate the effects of grid geometry variations on thruster discharge chamber performance. The dished grid parameters varied were: grid-to-grid spacing, screen and accelerator grid hole diameter, screen and accelerator open area fraction, compensation for beam divergence losses, and accelerator grid thickness. Also investigated were the effects on discharge chamber performance of main magnetic field changes, magnetic baffle current, cathode pole piece length and cathode position.

Introduction

Studies of solar electric propulsion systems show a need for 30-cm diameter mercury bombardment ion thrusters.[1,2] Overall efficiencies greater than 70 percent are desired at a maximum input power of approximately 2700 watts and a specific impulse of 3000 seconds. These requirements imply ion beam currents of about 2.0 amperes at net ion energies near 1100 volts from a discharge chamber with losses of about 200 eV per ion and a utilization efficiency greater than 95 percent. Thruster performance with dished grids presented in reference 3 was limited to 350 eV per ion at 95 percent utilization primarily because the screen grid open area was only 51 percent. References 4 through 8 have shown that the ion extraction system affects the thruster discharge chamber performance.

This paper presents the results of testing 13 sets of dished grids on five 30-cm thrusters in order to evaluate the effects of grid geometry changes on the discharge chamber performance. Use of an active magnetic baffle on three of the thrusters and main field electromagnets on one thruster allowed comparison of grid types at optimum thruster performance.

Apparatus and Procedure

Thrusters

Five different 30-cm thrusters, excluding the accelerator grid system, were used in this program and are described in Table 1. Thrusters A[4] and B[6] were optimized for use with composite grids whereas thruster C[9] was designed with a conventional flat 2-grid accelerator system. Tests using thruster C also utilized a separate power supply to excite the three turn magnetic baffle. The diameter of the physical baffle was varied from 4.13 to 5.25 cm. Thruster D was identical to thruster B with the following exceptions: (1) The 8 axial and 12 radial permanent magnets were replaced with 12 axial and 12 radial electromagnets with 270 and 300 turns, respectively, for each electromagnet. (2) The cathode-isolator-vaporizer assembly (CIV) for thruster D1 was taken from thruster C in order to use the magnetic baffle. Figure 1 is a sketch of the cathode assembly. Dimension "a" the position of the cathode tip with respect to the thruster backplate, normally 0.32 cm and dimension "b" was the length of the cathode pole piece, normally 5.08 cm. For thruster D1 the CIV had the dimensions listed above. For thruster D2 "b" was reduced to 2.54 cm by withdrawing the cathode assembly from the thruster. This made "a" equal to 2.2 cm upstream of the backplate. Thruster E was identical to thruster C except for the following modifications: (1) The axial and radial components of the magnetic field within the discharge chamber were increased. (2) For thruster E1 the dimensions "a" and "b" were the same as thruster D2. For thruster E2 the cathode tip, cathode keeper and magnetic baffle coil were moved 2.54 cm toward the baffle to locate the cathode tip at the original position. Dimensions "a" and "b" are listed in Table 1. For all tests the baffle was flush with the end of the cathode pole piece. Also listed in Table 1 are the distances from the baffle to the plane of the screen grid pole piece and the range of on-axis axial magnetic field strength from the baffle to the plane of the screen pole piece.

All thruster tests used hollow cathode neutralizers of the types described in references 6 and 10.

Ion Accelerator Systems

The grid sets listed in Table 2 and used in the program reported herein were fabricated from arc-cast molybdenum as described in reference 3. The aperture sizes, shapes, and spacings were varied as well as the dish depth. The grids were initially tested with insulating spacers of synthetic mica and then mounted on molybdenum rings for duration tests. The grids used in this program were mounted on the thruster dished away from the discharge chamber.

Facility and Power Supplies

All of the tests were conducted in the 3.0 m diameter bell jar of the 7.6 m diameter by 21.4 m long vacuum tank at the Lewis Research Center.[11] Power to the thrusters was supplied by laboratory power supplies. The magnet, the main discharge, the keeper and the positive and negative high voltage supplies were d.c. while the cathode tips and vaporizers were heated with 60 hertz a.c.

Magnetic Field Measurements

The axial and radial magnetic fields were measured with a Hall-effect gaussmeter using a three-dimensional probe. Magnetic field strengths were accurate to ±1 gauss.

Thruster Performance Evaluation

The thruster system was allowed to thermally stabilize at some upper value of discharge losses, ε_I, before the ε_I-propellant utilization, η_u, re-

lation was determined. Mercury flow rates were then obtained at fixed values of beam current, J_B, and discharge voltage, ΔV_I, usually 37 volts. The discharge current was reduced and the flow rates readjusted to give the previous value of J_B and ΔV_I. The values of η_u for the discharge chamber were not corrected for doubly charged beam ions or neutralizer flow rates. Cathode flow rates were held between 70 and 140 equivalent mA unless specified otherwise. All symbols are defined in the appendix.

Results and Discussion

As discussed in the Introduction, the ion accelerating systems of bombardment thrusters play an important role in determining the discharge chamber performance. Therefore a program was initiated to determine the effects of dished grid geometry changes on 30-cm thruster performance. As the program progressed, it was found that there were considerable interactions between grid geometry changes and thruster changes. As an example of these interactions, figure 2 compares the discharge chamber performance of the five thrusters of table 1 when tested with grid set F and the grids for which thrusters A, B, and C were optimized. It can be seen that there was considerable degradation in the performance of thrusters A and B when grid set F replaced the composite grids. The performance of thruster C improved when it was operated with dished grids even though ΔV_I was 3 volts less than reported for flat grid operation. The maximum discharge chamber performance for grid set F occurred when those grids were tested on thruster D1, an electromagnet thruster with an active magnetic baffle. In that test the main magnetic field was optimized for maximum discharge chamber performance.

Figure 2 shows that to justly evaluate the effects of grid geometry changes on thruster performance, it is necessary to have that thruster be of the optimum configuration for that particular grid set.

The balance of this section presents the effects on discharge chamber performance of variations in the grid geometry, main magnetic field, magnetic baffle and the cathode assembly.

Ion Accelerating System

The desired flexibility of an electromagnet thruster was not always available because five different thrusters were used in this grid evaluation program. Therefore, the results of grid geometry changes presented below should be used only to indicate relative and not necessarily absolute thruster performance gains.

Grid-to-grid spacing. Past ion thruster tests have shown that the ε_I could be reduced by increasing the total grid voltage or decreasing the grid-to-grid spacing.[3,7,12] This was attributed to movement of the sheath at the screen grid toward the discharge chamber thereby increasing the effective open area of the screen grid and extracting more ions from the plasma. To determine the sensitivity of the discharge chamber performance on grid spacing, several tests were conducted over a wide range of spacings. Figure 3(a) shows an improvement in the discharge chamber performance of thruster C for grid sets B, C, and E (identical except for compensation and spacing) with a screen grid open area fraction, F_{OS}, of 0.51 as the cold grid spacing was decreased from 1.09 to 0.84 and 0.63 mm. However, it is seen that the sensitivity of discharge chamber performance to grid spacing decreased as the spacing decreased. Reference 3 also reported nearly constant discharge chamber performance for identical grids with spacings of 0.86 and 0.66 mm tested on thruster B. Figure 3(b) shows the discharge chamber performance for thruster E2 with grid sets J and H (F_{OS} equal to 0.67) having grid spacings of 0.51, 0.74, and 0.92 mm. Again the performance variations were negligible. Figure 3(c) also shows almost no variation in discharge chamber performance as the grid spacing was varied from 0.92 to 1.30 to 1.98 mm for grid set N tested on thruster C. The F_{OS} for grid set N was 0.77.

In general, for grids with F_{OS} of 0.51 and spacings less than 0.84 mm and grids with F_{OS} of 0.67 and 0.77 at any spacing up to 1.98 mm, the discharge chamber performance for a given grid geometry and given thruster was insensitive to grid spacing. This can be explained as follows. The effective screen grid hole diameter is larger than the physical hole diameter and increases with decreasing grid spacing for grids with F_{OS} of 0.51. As F_{OS} is increased the effective hole diameters of adjacent holes probably come into contact with each other thereby limiting the effective F_{OS} to a value near unity. For the grid spacings and voltages of interest, all operation of grids with F_{OS} of 0.67 and 0.77 was probably near the maximum effective F_{OS} and therefore insensitive to changes in grid spacing. This also implies that for a particular thruster and its plasma density profile, the ion extraction was near maximum. One way to increase the ion extraction efficiency would be to flatten the plasma profile as suggested in reference 13.

For most of the grid geometries tested, the thruster performance was insensitive to grid spacing changes for a given grid geometry. Therefore, the effects of different grid geometries on discharge chamber performance of any given thruster could be evaluated.

d_S and d_A increase, F_{OS} and F_{OA} constant. Several grid sets with F_{OS} of 0.51 and 0.67 and F_{OA} of 0.43, 0.51, and 0.67 with varying hole diameters were tested on thruster C. Figure 4(a) shows the discharge chamber performance of thruster C with grid sets A and C. The open area of both grids of each set was 0.51 but the grid hole diameters for grid set A were 1.02 mm and for grid set C were 1.91 mm. Both the maximum η_U and the minimum ε_I were larger for the test with the small holes. The larger holes of grid set C may allow deeper penetration of the plasma sheath into the discharge chamber resulting in a larger extraction area and lower ion losses at the screen grid.

In figures 4(b) and (c) where F_{OS} was 0.67 for all grid sets there were no significant differences in the discharge chamber performance as the d_S was varied from 1.91 to 2.41 mm. Apparently this resulted because operation was always at the maximum effective open area. The improved performance shown in figure 4(c), relative to that of 4(a)

and (b), can be attributed to higher F_{OS} and lower F_{OA} in the first case and lower F_{OA} and higher ΔV_I in the second case.

F_{OS} and F_{OA} increase, d_S and d_A constant. Starting with the grid geometry of reference 3, where the F_{OS} and F_{OA} were 0.51 and the hole diameters were 1.91 mm, the F_{OS} and F_{OA} were increased to 0.67 with the same hole diameters by decreasing the center-to-center hole spacing.

Figures 5(a) and (b) show the discharge chamber performance of thrusters C and E2 with grid sets C and F and D and F, respectively. In both cases, as the F_{OS} and F_{OA} were increased from 0.51 to 0.67 the minimum ε_I decreased about 15 percent while the maximum η_U decreased about 2 percent. The discharge chamber losses probably decreased because there was less screen grid surface on which ions could be lost (larger effective open area). But at the same time, some of the neutral mercury atoms which were contained by the initially low F_{OS} were lost as F_{OS} was increased causing the degradiation in η_U.

d_A and F_{OA} decrease, d_S and F_{OS} constant. Two grid sets with F_{OS} and F_{OA} of 0.67 were compared with two other grid sets with F_{OS} of 0.67 and F_{OA} of 0.43. The comparisons were made on thruster C for grids with d_S of 1.91 and 2.41 mm. In both cases when F_{OA} was reduced, the η_U increased for all ε_I. In particular, figure 6(a) shows that at the knee of the curve the η_U increased about 3 percent as the F_{OA} was reduced.

Figure 6(b) shows a similar effect when grid sets G and M, both with d_S of 2.41 mm but with d_A of 2.41 and 1.93 mm, respectively, were tested on thruster C. Here the thruster performance improvement was partly due to the fact that a separate magnetic baffle power supply was used when d_A was reduced, allowing the cathode flow rate to be decreased, which resulted in a η_U increase of about 2 percent. Thus, the improvement in η_U due only to the reduction of d_A, was about 4 percent. The thruster performance of figure 6(b) was degraded from that of 6(a) because the ΔV_I was 35 volts for 6(b) and 37 volts for 6(a).

The thruster performance improvements resulting from the decrease of d_A were most likely caused by the increased reflection of neutral mercury atoms.

Compensated grids. Hole pattern compensation of dished grids is required to reduce the inherent thrust losses due to beam divergence discussed in references 3 and 14. The center-to-center hole spacing was either increased for the accelerator grid or decreased for the screen grid. The amount of compensation was measured as a strain and was equal to the ratio of the change in spacing to the original spacing.

It was desirable to determine if compensation of grids affected the discharge chamber performance. Figure 7 shows that the discharge chamber performance for two different grid geometries tested on thrusters C and D2 was not affected by grid compensation.

Accelerator grid thickness. The minimum total accelerating voltage required to extract a 2.0 ampere beam from dished grids is approximately 1200 volts. An effective specific impulse of 3000 seconds requires a net accelerating voltage of approximately 1100 volts. The negative voltage of the accelerator grid is primarily required to prevent electron backstreaming rather than add to the total accelerating voltage and is of the order 300 to 500 volts. At these relatively low voltages the accelerator lifetime has been greatly extended. Therefore, the accelerator thickness was reduced from 0.76 to 0.51 mm. Grid sets H and J were tested on thruster E2 to determine the effect, if any, on thruster performance of accelerator grid thickness. Figure 8 shows that there was no change in performance when the accelerator grid thickness was reduced.

Main Magnetic Field

The on-axis values of axial magnetic field strength at the baffle and the plane of the screen grid pole piece are listed in Table 1 for thrusters A, B, C, and E. The reference point for the axial position was chosen to be the baffle because it was the upstream boundary of the primary electron region of the discharge chamber.[15] The position of the downstream boundary (screen grid) was a function of the shape of the grid used. The location of the plane of the screen grid pole piece is also indicated in Table 1. The magnetic field strength as well as the volume of the primary electron region was increased when going from thruster A to E. The higher on-axis field strengths obtained near the baffle with thrusters C and E are caused by the presence of the magnetic baffle. Away from the baffle, the stronger fields were attributed to a greater number of permanent magnets.

References 6, 13, and 16 have shown that the strength and shape of the magnetic field within the discharge chamber can have a strong affect upon the discharge chamber performance. Therefore, it is desirable to be able to change the magnetic field strength and shape during the evaluation of thruster performance for each component variation. This was accomplished with thruster D which had separately excited axial and radial electromagnets. To observe the effects of the magnet currents on the beam current, the discharge current, accelerating voltages and mercury flow rates were held constant while one of the magnet currents was varied. The other magnet current was held constant at its optimum value. The magnetic baffle current was varied to maintain a constant discharge voltage. Figure 9 shows the variation of beam current with either the axial or radial magnet current for grid set J on thruster D2 at approximately 2650 watts of input power. The shapes of the curves were typical for other levels of input power and for other grids tested on this thruster. The beam current always increased rapidly with either magnet current up to some fairly well defined value after which it was nearly constant for increasing magnet currents. This optimum value of magnet current increased with input power or beam current. For input powers of 2000 and 1400 watts, the optimum magnet currents were 0.8 and 0.6 amperes, respectively.

Figure 2 showed an improvement in thruster performance when grid set F was operated on thruster D1 rather than thruster C. The performance

shown for thruster D1 was obtained at the optimum axial and radial magnet currents. Figure 10 also compares the performance of thrusters C and D1 when grid sets J and N were used. In both tests thruster performance increased when the main magnetic field was optimized. The difference in performance between the two grid sets was significantly less on thruster D1 than on thruster C, thereby showing again the need for a flexible thruster when comparing two grids with different geometries.

Magnetic Baffle

References 14, 17, and 18 have shown that the magnetic baffle aids in the control of electron flow from the hollow cathode to the anode of 30-cm diameter thrusters thereby allowing increases in thruster performance and throttling range. The discharge voltage was reduced when either the physical baffle diameter or magnetic baffle ampere-turns was decreased.[17,19] The reduction of ΔV_I, caused by either a physical or magnetic baffle reduction, can be negated by a decrease in cathode flow rate. Reference 17 has indicated that optimum performance for single point operation is obtained with the minimum permissible cathode flow.

Figure 11 shows the variation of discharge chamber performance with magnetic baffle current, J_{MB}, for thruster C. The cathode flow rate, J_{OK} in equivalent mA, is listed at each data point. The overall discharge chamber performance increased monotonically with decreasing J_{MB} (or J_{OK}). This trend was observed with all thrusters and grid combinations presented herein. The lower limit of J_{MB} or J_{OK} was reached when the discharge instability mentioned in references 17 and 18 was observed. As the J_{OK} was reduced from a high value (approx. 200 mA), the ΔV_I would gradually increase to some relative maximum value, rapidly decrease about 10 volts, and then increase until the discharge would extinguish. A decrease in J_{MB} would decrease the relative maximum value of ΔV_I. The minimum J_{MB} was that value which caused the relative maximum of ΔV_I to be slightly greater than the desired ΔV_I.

The flexibility of the magnetic baffle is further shown in figure 12 which presents the performance of thruster C when tested with three different physical baffles having diameters of 4.13, 4.76, and 5.25 centimeters. At each data point, the magnetic baffle current was reduced to the lowest value which gave stable thruster operation. Figure 12 shows that the same discharge chamber performance was obtained regardless of the baffle diameter as long as the magnetic baffle was used to minimize the cathode flow rate. Thus, by using a separate power supply to excite the magnetic baffle coil the η_U can be maximized at any ϵ_I or J_B for any particular combination of thruster, grid set, magnetic field, cathode geometry, and baffle diameter.

Cathode Assembly Variations

Cathode pole piece length. As mentioned earlier, the main magnetic field strength and shape affects the thruster performance. Therefore, four different cathode pole piece lengths were tested in thruster D using grid set F with the intent of improving the magnetic field shape of a thruster which was optimized for flat grids. The standard cathode assembly (including cathode, isolator, vaporizer, cathode pole piece, magnetic baffle, and excitation coil) was moved as a unit in and out of the thruster to obtain the variations in cathode pole piece length ("b" in fig. 1). Figure 13 shows that the discharge chamber performance improved as the cathode assembly was retracted from 7.62 cm into the discharge chamber to 2.54 cm. When the cathode assembly was retracted such that the pole piece length was only 0.32 cm performance degraded slightly. For each configuration the axial, radial, and magnetic baffle electromagnets were varied to obtain the maximum performance. The improvement in the discharge chamber performance obtained with the shorter pole piece was probably due to an improved magnetic field shape as well as the higher field strength required for optimum operation with dished grids.

Figure 14 shows the discharge chamber performance for grid set J, with F_{0A} of 0.43, on thruster D with the pole piece at the 5.08 cm position. Again a small improvement, relative to figure 13, in the propellant utilization was realized due to the decrease in F_{0A}. Another performance gain occurred, as in figure 13, when the cathode assembly was retracted to the 2.54 cm position. The optimum magnetic field shape and strength of thruster D was duplicated on thruster E1 with permanent magnets and the discharge chamber performance remained unchanged.

Cathode position. When the standard cathode assembly was retracted 2.54 cm, as explained above, the cathode tip was then about 2.2 cm ("a", fig. 1) upstream of the plane of the propellant distributor backplate. This cathode position was physically and thermally undesirable so the cathode tip magnetic baffle coil and cathode keeper were moved downstream to the original position and only the physical baffle and cathode pole piece were retracted 2.54 cm. This resulted in a decrease of ϵ_I as shown in figure 14. References 19 and 20 have also shown that the discharge chamber performance of a 15 cm thruster was affected by cathode position.

Summary of Discharge Chamber Optimization

Figure 15 summarizes the gains in discharge chamber performance as thruster C with flat grids evolved to thruster E2 with dished grids. Shown is the discharge chamber performance of thruster C tested with flat grids, with dished grid set F, and with grid set J. Also shown is the performance of thruster E2 (thruster C with modifications presented in the previous section) operated with grid set J. At a η_U of 0.93 the discharge losses were decreased by 70 eV per ion with the addition of grid set J to thruster C. At an ϵ_I of 190 the thruster modifications resulted in a η_U increase of 5 percent.

Table 3 compares the discharge chamber performance of thruster C with flat grids[9] and thruster E2 with grid set J operated at three different levels of input power. The performance improved with the modified thruster using dished grids not only at full power as shown in figure 15 but at power inputs of three-fourths and half of full power.

Conclusions

The effects of dished grid geometry on the discharge chamber performance have been presented. Five different 30-cm diameter thrusters were used to evaluate 13 different sets of grids with 13 different grid geometries. It was found that, in all cases, to obtain the maximum thruster performance, the discharge chamber should be optimized for the particular grid set which would finally be used. A thruster which was optimized for a flat two-grid accelerating system was operated with dished grids at lower discharge losses and higher propellant utilizations. The improvements in discharge chamber performance, experienced over a two-to-one throttling range, were attributed to the dished grids, a stronger main magnetic field, cathode assembly modifications, and an optimized cathode flow rate.

The variations of dished grid geometries and the generalized results are summarized below:

1. For dished grids with a F_{OS} of 0.51 and a grid-to-grid spacing of less than 0.84 mm or grids with the F_{OS} greater than 0.67 at any spacing, the discharge chamber performance of any thruster was insensitive to the grid spacing. This apparently occurred because the effective open area of the screen grid reached a constant maximum value when the above conditions were met thereby fixing the ion transmission of the grids. This fact allowed most of the grid geometry changes to be compared even at different grid-to-grid spacings.

2. For grid sets with the F_{OS} and F_{OA} equal to 0.51, the minimum ε_I and the maximum η_U decreased as the grid hole diameter increased. Again, it is probable that the effective open area of the screen grid was larger for the larger holes, therefore ε_I and η_U decreased. For grid sets with F_{OS} equal to 0.67 there was no change in performance as the grid hole diameters were varied.

3. For all of the grids tested, when the F_{OS} and F_{OA} were increased the minimum ε_I decreased as well as the η_U. With a greater effective F_{OS} the ions in the discharge chamber were more efficiently extracted, but the larger F_{OA} also allowed a greater number of neutral atoms to be lost.

4. When the F_{OA} was decreased while F_{OS} was held constant the η_U always increased for all ε_I. The η_U increased because some of the neutral atoms passing through the screen grid were reflected by the smaller accelerator holes.

5. There was no change in the discharge chamber performance of thrusters equipped with grids which were compensated to minimize the thrust loss due to beam divergence.

6. There was no change in the discharge chamber performance when the thickness of the accelerator grid was reduced from 0.76 to 0.51 mm.

It was found to be desirable to be able to change the magnetic field strength and shape during the evaluation of thruster performance for thruster component variation. This was accomplished by using a thruster with electromagnets to generate the main magnetic field.

When a separate power supply was used to excite the magnetic baffle of thruster C the cathode flow could be minimized at any thruster condition to give the maximum discharge chamber performance.

The discharge chamber performance was noted to be a function of the cathode pole piece length probably because it changed the main magnetic field to a more desirable shape. The cathode position also affected thruster performance.

The discharge chamber performance of the 30-cm diameter thruster with dished grids has surpassed that of the thrusters with composite grids yet dished grids offer the extended lifetime of previously tested two-grid accelerating systems.

Appendix - Symbols

B_Z axial magnetic field strength, gauss

d_A accelerator grid hole diameter, mm

d_S screen grid hole diameter, mm

F_{OA} accelerator grid open area fraction

F_{OS} screen grid open area fraction

J_B beam current, amp

J_I discharge current, amp

J_{MB} magnetic baffle current, amp

J_{OK} cathode propellant flow rate, equiv. mA

V_A accelerator voltage, V

V_I net ion accelerating voltage, V

ΔV_I discharge voltage, V

ε_I discharge chamber energy per beam ion, eV/ion

η_U propellant utilization efficiency

References

1. Gardner, J. A., "Solar Electric Propulsion System Integration Technology (SEPSIT). Vol. III: Supporting Analyses," TM 33-583, NASA CR-130703. Nov. 1972, Jet Propulsion Lab., Pasadena, Calif.

2. Anon., "Study of a Common Solar-Electric-Propulsion Upper Stage for High-Energy Unmanned Missions. Vol. 2: Technical," Rep. TRW-16552-6007-RO-00-Vol. 2, NASA CR-114350, July 1971, TRW Systems Group, Redondo Beach, Calif.

3. Rawlin, V. K., Banks, B. A., and Byers, D. C., "Dished Accelerator Grids on a 30-cm Ion Thruster," Journal of Spacecraft and Rockets, Vol. 10, No. 1, Jan. 1973, pp. 29-35.

4. Bechtel, R. T., "Performance and Control of a 30-Cm-Diam, Low-Impulse, Kaufman Thruster," Journal of Spacecraft and Rockets, Vol. 7, No. 1, Jan. 1970, pp. 21-25.

5. Bechtel, R. T., "Component Testing of a 30-Centimeter Diameter Electron Bombardment Thruster," Paper 70-1100, Sept. 1970, AIAA, New York, N.Y.

6. King, H. J., and Poeschel, R. L., "Low Specific Impulse Ion Engine," NASA CR-72677, Feb. 1970, Hughes Research Labs., Malibu, Calif.

7. Byers, D. C., "An Experimental Investigation of a High-Voltage Electron-Bombardment Ion Thruster," Journal of the Electrochemical Society, Vol. 116, No. 1, Jan. 1969, pp. 9-17.

8. Bechtel, R. T., "Discharge Chamber Optimization of the SERT II Thruster," Journal of Spacecraft and Rockets, Vol. 5, No. 7, July 1968, pp. 795-800.

9. Anon., "Low Voltage 30-cm Ion Thruster," NASA CR-120919, Feb. 1972, Hughes Research Lab., Malibu, Calif.

10. Bechtel, R. T., "A Hollow Cathode Neutralizer for a 30-cm Diameter Bombardment Thruster," AIAA paper to be presented at the 10th Electric Propulsion Conference, Oct. 31-Nov. 2, 1973.

11. Finke, R. C., Holmes, A. D., and Keller, T. A., "Space Environment Facility for Electric Propulsion Systems Research," TN D-2774, 1965, NASA, Cleveland, Ohio.

12. Pawlik, E. V., Margosian, P. M., and Staggs, J. F., "A Technique of Obtaining Plasma-Sheath Configurations and Ion Optics from Electron Bombardment Ion Thruster," TN D-2804, 1965, NASA, Cleveland, Ohio.

13. Knauer, W., Poeschel, R. L., King, H. J., and Ward, J. W., "Discharge Chamber Studies for Mercury Bombardment Ion Thrusters," NASA CR-72440, Sept. 1968, Hughes Research Labs, Malibu, Calif.

14. Danilowicz, R. L., Rawlin, V. K., Banks, B. A., and Wintucky, E. G., "Measurement of Beam Divergence of 30-cm Diameter Dished Grids," AIAA paper to be presented at the 10th Electric Propulsion Conference, Oct. 31-Nov. 2, 1973.

15. Kaufman, H. R., "Ion Thruster Propellant Utilization," Journal of Spacecraft and Rockets, Vol. 9, No. 7, July 1972, pp. 511-517.

16. Bechtel, R. T., "Discharge Chamber Optimization of the SERT II Thruster," Journal of Spacecraft and Rockets, Vol. 5, No. 7, July 1968, pp. 795-800.

17. Bechtel, R. T., "A 30-cm Diameter Bombardment Thruster with a Variable Magnetic Baffle," Paper 72-489, Apr. 1972, AIAA, New York, N.Y.

18. Poeschel, R. L., "The Variable Magnetic Baffle as a Control Device for Kaufman Thrusters," Paper 72-488, Apr. 1972, AIAA, New York, N.Y.

19. Bechtel, R. T., Csiky, G. A., and Byers, D. C., "Performance of a 15-cm Diameter Hollow-Cathode Kaufman Thruster," Paper 68-88, Jan. 1968, AIAA, New York, N. Y.

20. Wilbur, P. J., "Experimental Investigation of a Throttlable 15-cm Hollow Cathode Ion Thruster," NASA CR-121038, Dec. 1972, Dept. of Mechanical Engineering, Colorado State University, Fort Collins, Colo.

Table 1. Thruster description

Thruster	Basic thruster design	Thruster modifications	Cathode pole piece length WRT thruster backplate, cm	Cathode tip position WRT thruster backplate, cm	Range of B_Z from baffle to plane of screen pole piece, gauss	Distance from baffle to plane of screen pole piece, cm
A	LeRC (ref. 4)	None	5.08 downstream	0.0 downstream	17-7	6.3
B	HRL300 (ref. 6)	None	5.08	.0	26-7	9.6
C	HRL400 (ref. 9)	Active magnetic baffle	5.08	.32	56-10	9.6
D1	HRL300	Active magnetic baffle, axial and	5.08	.32		9.6
D2		radial electromagnets	2.54	2.2 upstream		
E1	HRL400	Active magnetic baffle, cathode pole	2.54	2.2 upstream	62-8	12.2
E2		piece shortened, stronger magnetic field	2.54	.32 downstream		

Table 2. Dished grid geometry

Grid set	Hole diam., mm		Grid thickness, mm		Open area fraction		Compensation, percent strain	Aperture shape	Ratio of dish depth to dish diameter
	Screen	Accelerator	Screen	Accelerator	Screen	Accelerator			
A	1.02	1.02	0.38	0.38	0.51	0.51	0	Circular	0.075
B	1.91	1.91					0		
C							.22		
D							.44		
E							.66		
F					.67	.67	0		
G	2.41	2.41				.67	0		
H	1.91	1.52		.51		.43	0		
J	1.91	1.52		.76			0		
K	1.91	1.52					.35		
L	2.16	1.73					0		
M	2.41	1.93					0		
N	2.08	2.08		.38	.77	.77	.097	Hexagonal	.038

Table 3. Thruster performance comparison

Thruster description	Input power, watts	Net ion accelerating voltage, V	Beam current, amps	Discharge chamber losses, eV/ion	Propellant utilization efficiency
Thruster C	2577	1000	2.0	260	0.976
Flat grids	1969	1000	1.55	255	.899
(ref. 9)	1258	1000	0.95	271	.727
Thruster E2	2610	1100	2.03	180	.971
Grid set J	1950	1225	1.36	160	.892
	1384	1350	.87	177	.822

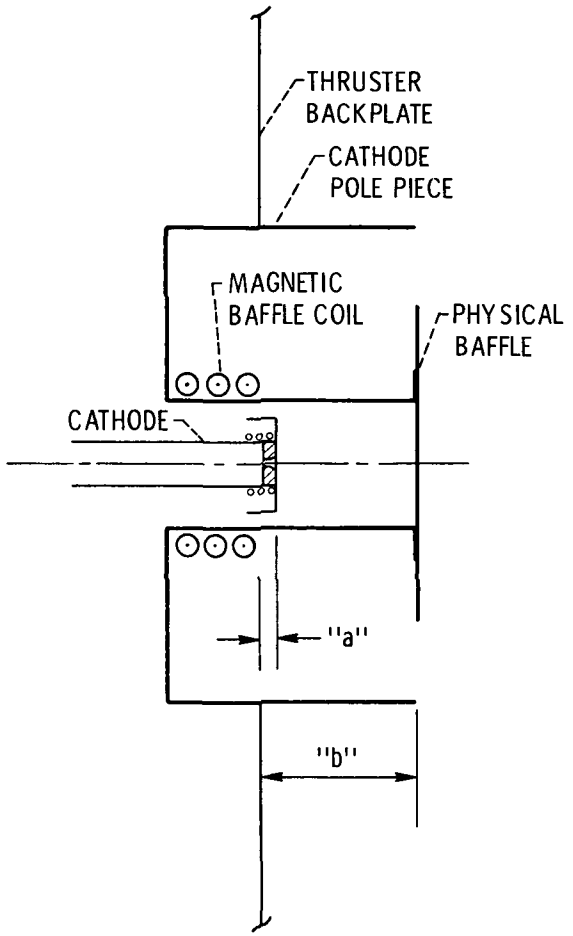

Figure 1. - Thruster C cathode assembly.

	GRID USED	V_I, v	J_B, a	V_A, v	ΔV_I, v
———	F, TABLE II	1000-1100	2.0	500	37
—·—	COMPOSITE REF. 6	1000	1.85	~800	~40
– – –	COMPOSITE REF. 4	600	1.5	550	40
o	FLAT 2 GRID REF. 9	1000	2.0	1500	42

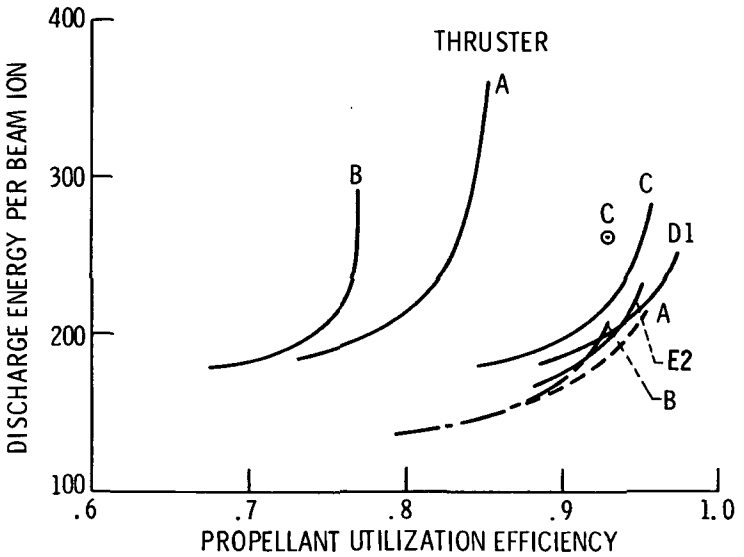

Figure 2. - Comparison of discharge chamber performance for the thrusters of Table I operated with several grids.

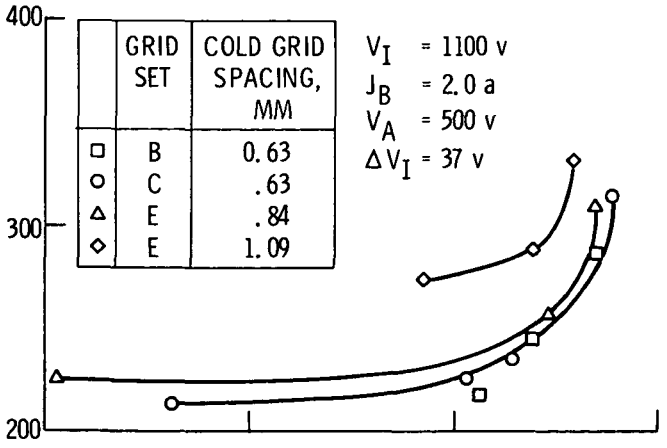

(a) F_{OS} = 0.51, THRUSTER C.

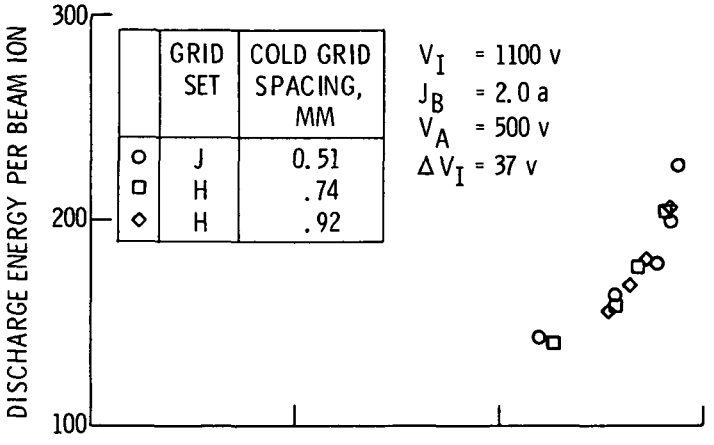

(b) F_{OS} = 0.67, THRUSTER E2.

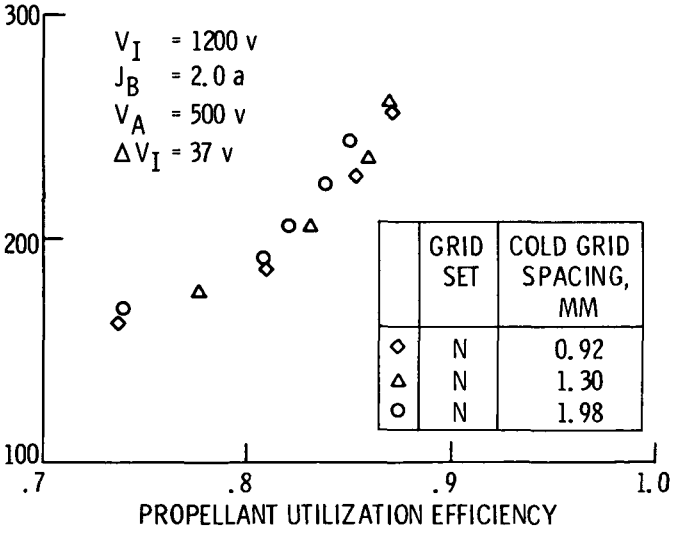

(c) F_{OS} = 0.77, THRUSTER C.

Figure 3. - Discharge chamber performance variation with grid spacing.

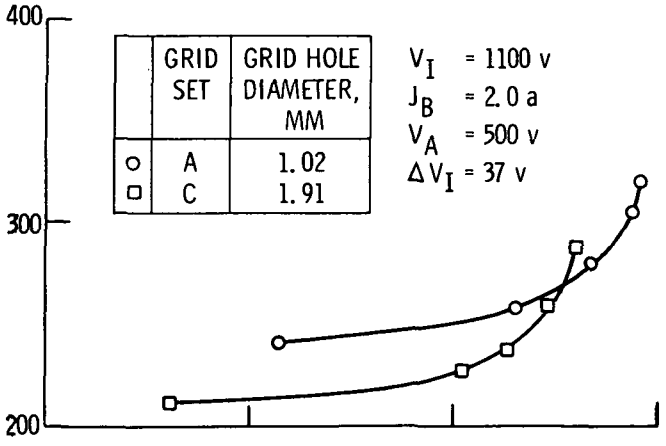

(a) F_{OS} = 0.51, THRUSTER C.

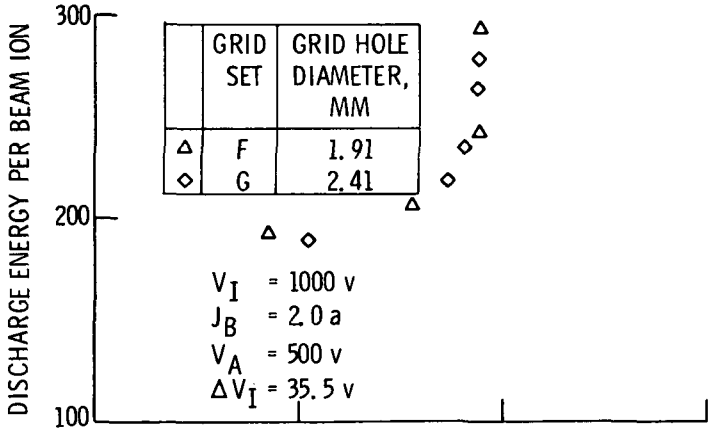

(b) F_{OS} = 0.67, THRUSTER C.

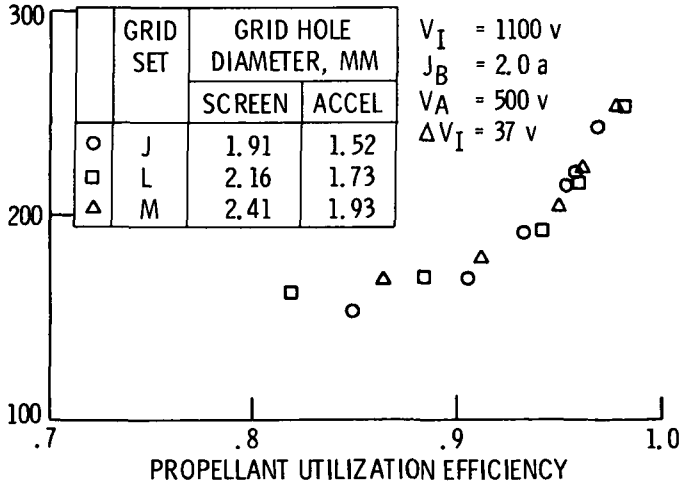

(c) F_{OS} = 0.67, THRUSTER C.

Figure 4. - Discharge chamber performance variation with grid hole diameter.

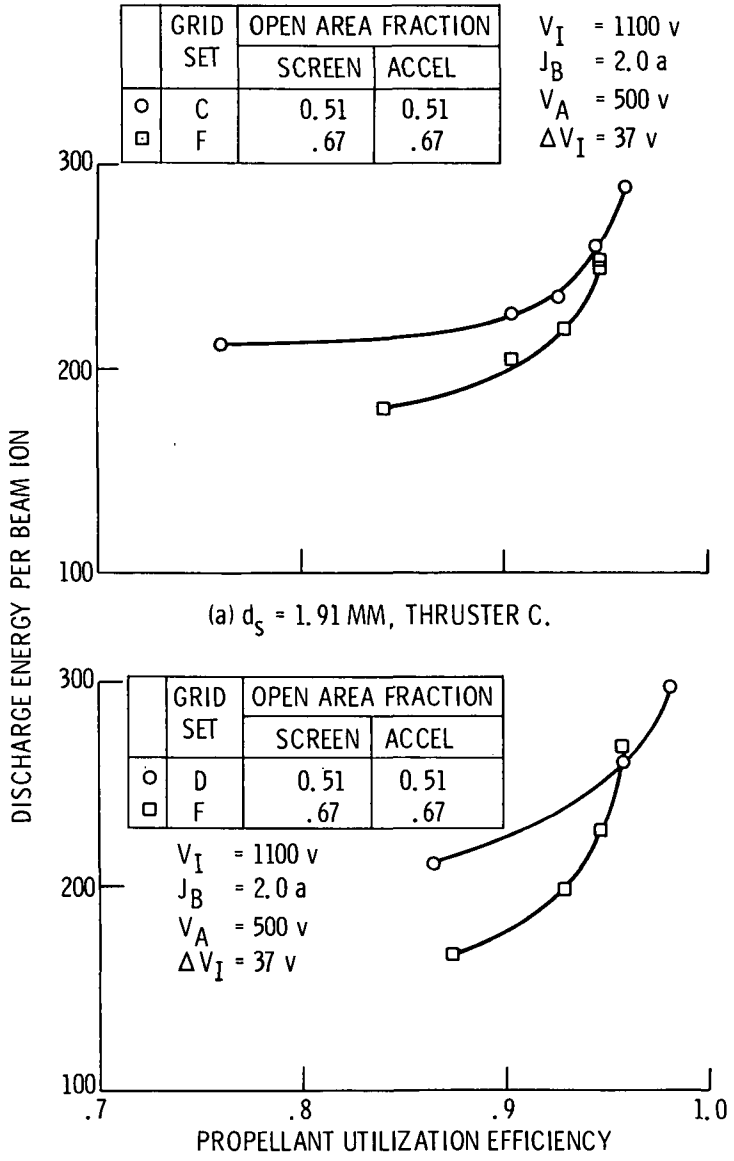

Figure 5. - Discharge chamber performance variation with grid open area fraction.

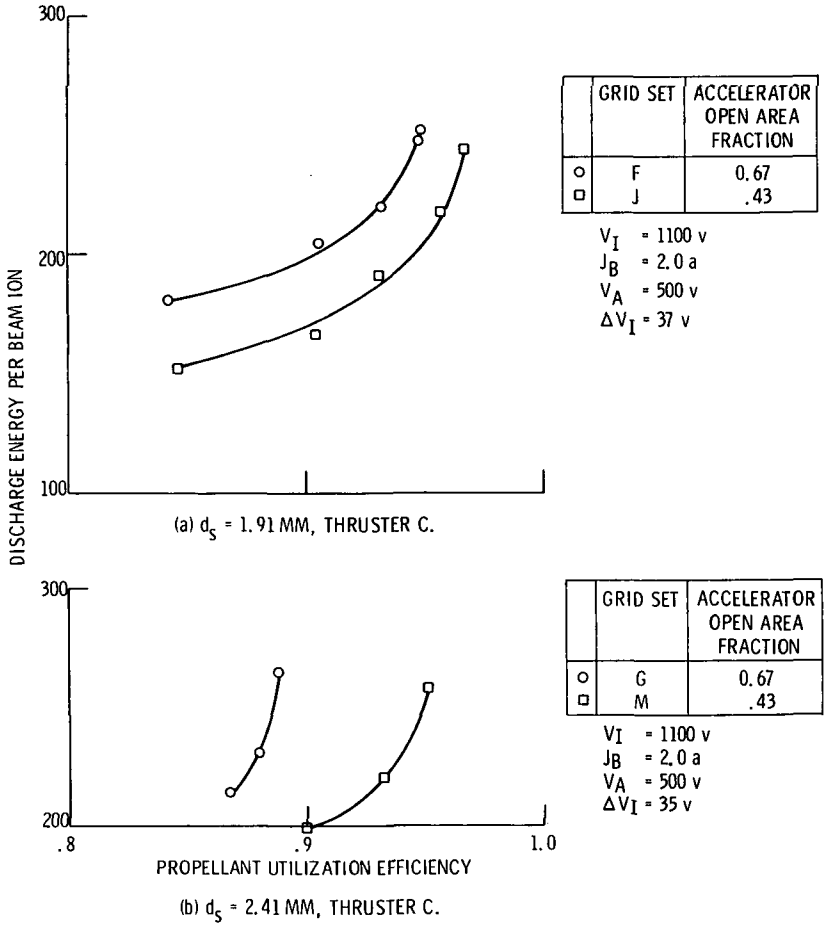

Figure 6. - Discharge chamber performance variation as accelerator open area fraction decreases.

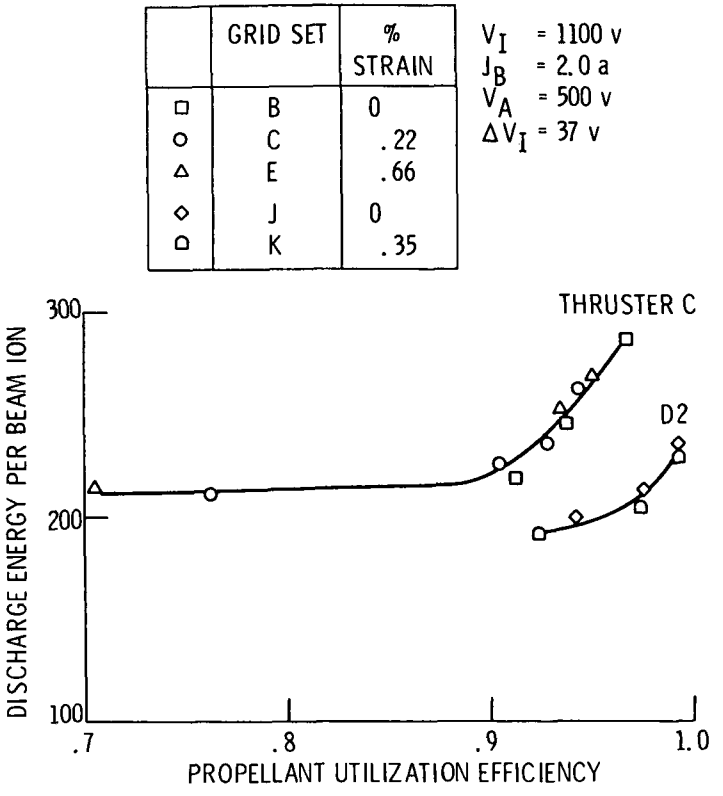

Figure 7. - Discharge chamber performance variation for compensated grids.

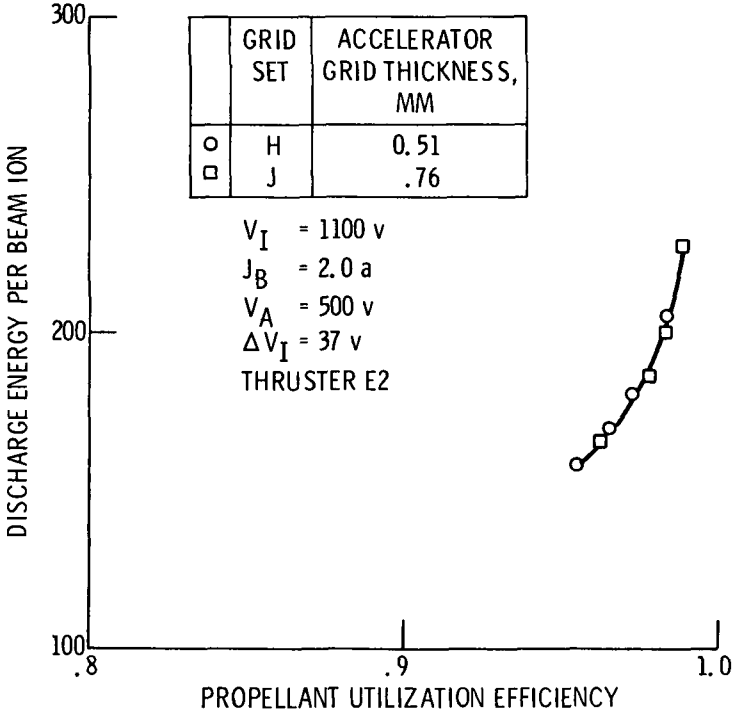

Figure 8. - Discharge chamber performance variation with accelerator grid thickness.

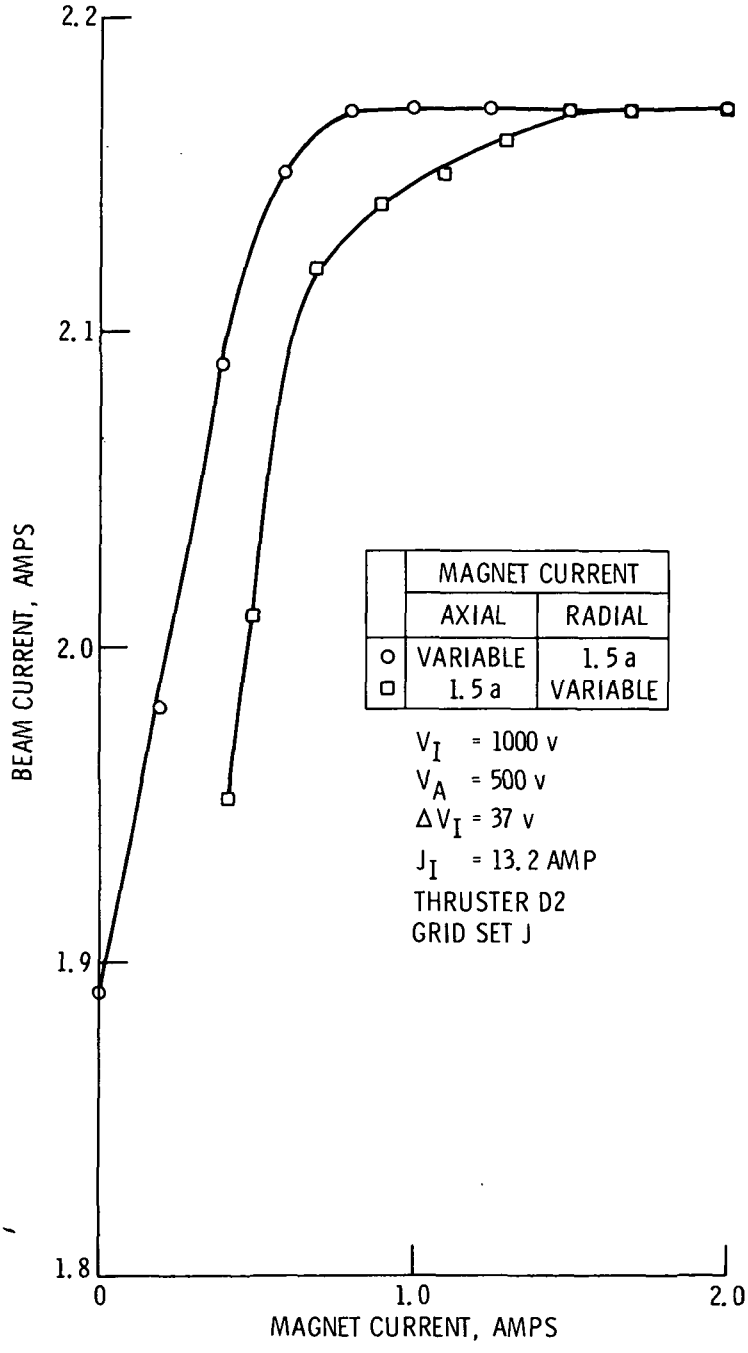

Figure 9. - Variation of beam current with current through electromagnets.

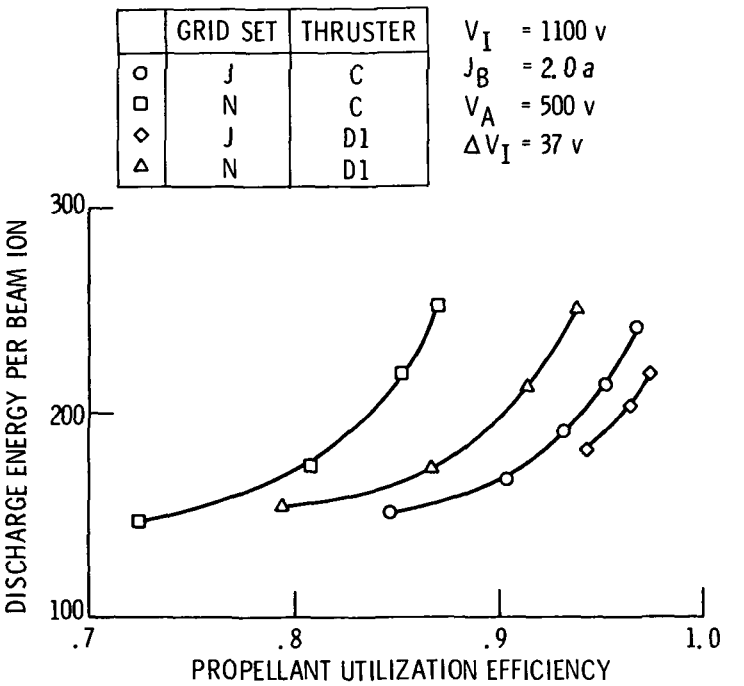

Figure 10. - Comparison of discharge chamber performance of thrusters C and D1 with grid sets J and N.

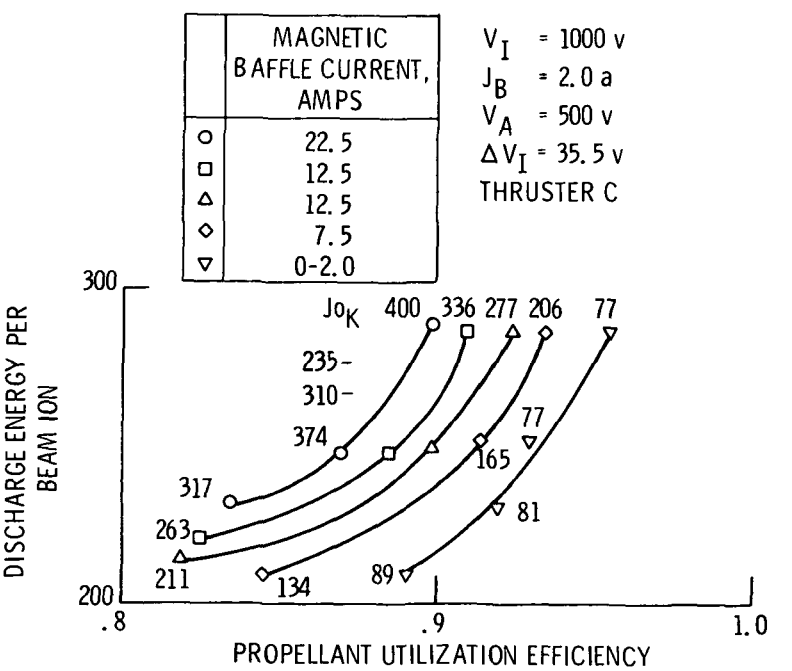

Figure 11. - Discharge chamber performance variation with magnetic baffle current.

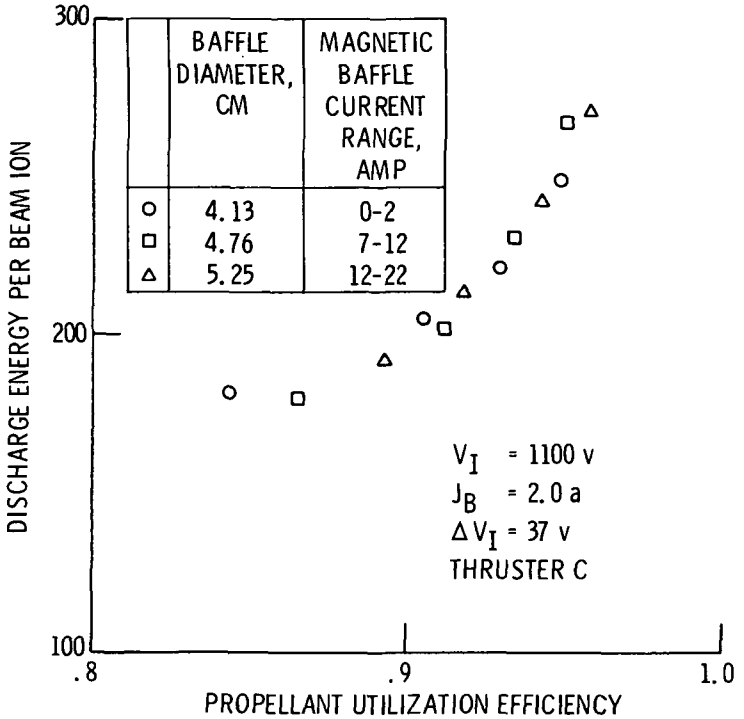

Figure 12. - Discharge chamber performance variation with baffle diameter.

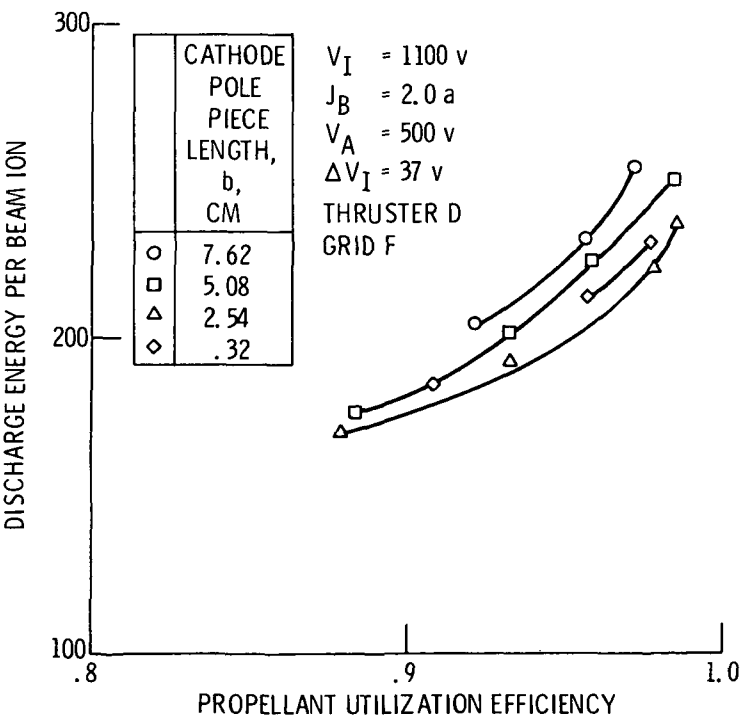

Figure 13. - Discharge chamber performance variation with cathode pole piece length.

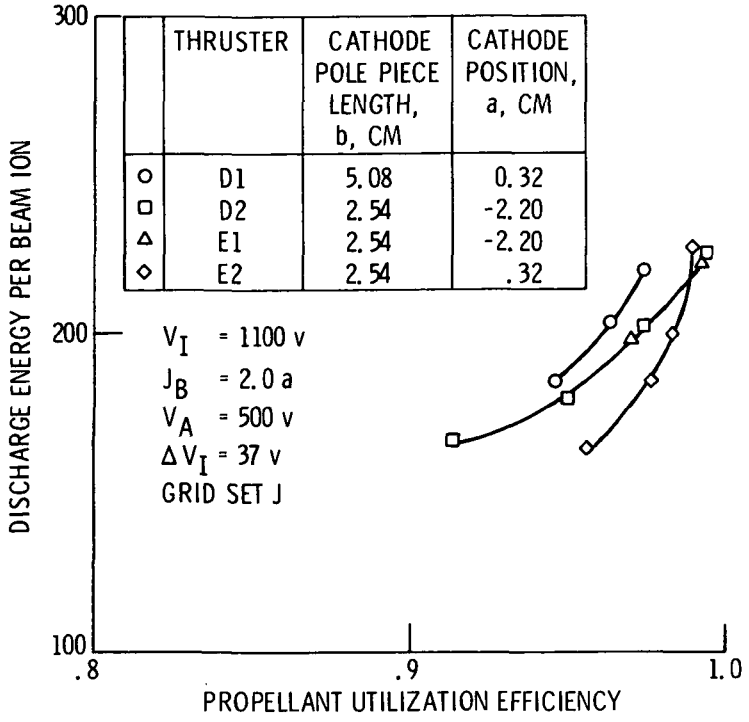

Figure 14. - Discharge chamber performance variation with cathode position.

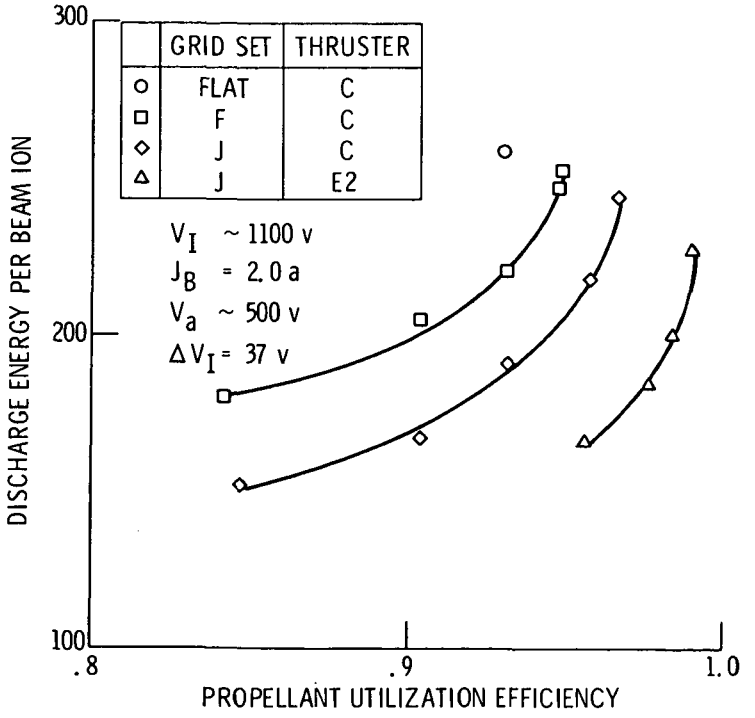

Figure 15. - Summary of thruster performance optimization.